ARTICLE

m6A-modified circFOXA1 promotes tumor immune evasion via enhancing PD-L1 deubiquitination in triple-negative breast cancer

Honghong Shen · Boyu Li · Xiaoqian Wen · Changqing Zhao · Chen Wang

Received: 9 February 2026 / Accepted: 1 April 2026

Abstract

Restoring $CD8^+$T cell infiltration and potentiating anti-tumor immune responses in the tumor microenvironment (TME) is critical for developing effective immunotherapies against triple-negative breast cancer(TNBC), while the regulatory role of N^6-methyladenosine (m^6A)-modified circular RNAs (circRNAs) in TNBC immune escape remains largely unelucidated. Whole-transcriptome microarray analysis combined with bioinformatics mining was conducted on TNBC tissues to screen circRNAs associated with immune evasion. RNA immunoprecipitation (RIP), RNA pulldown, and methylated RNA immunoprecipitation (MeRIP) assays were performed to verify the m^6A modification of circFOXA1 and its interaction with gasdermin C (GSDMC). In vitro T cell-mediated tumor cytotoxicity assays and in vivo xenograft models in C57BL/6 mice were used to investigate the functional roles of the circFOXA1/GSDMC axis in TNBC anti-tumor immunity. Luciferase reporter and actinomycin D assays were further applied to clarify the regulatory mechanism of GSDMC on OTUB1 and programmed cell death-ligand 1 (PD-L1) expression. CircFOXA1 was identified as an m^6A-modified circRNA with high stability and upregulation in TNBC, and its expression was significantly negatively correlated with $CD8^+$T cell infiltration in TNBC tissues. Functionally, circFOXA1 induced immunosuppression in a $CD8^+$T cell-dependent manner both in vitro and in vivo. Mechanistically, the m^6A writer METTL14 mediated the m^6A modification of circFOXA1, and the m^6A reader YTHDF2 promoted circFOXA1 circularization. CircFOXA1 impaired immune cell-dependent tumor killing by upregulating GSDMC expression, which further enhanced OTUB1 mRNA stability at the post-transcriptional level. OTUB1-mediated deubiquitination subsequently stabilized PD-L1 protein, ultimately inhibiting $CD8^+$T cell infiltration and driving TNBC immune escape. This study identifies a novel regulatory axis of m^6A-modified circFOXA1/GSDMC/OTUB1/PD-L1 in mediating TNBC immune escape, where GSDMC enhances PD-L1 protein stability via OTUB1-dependent deubiquitination. These findings reveal a new molecular mechanism underlying TNBC immune evasion and identify circFOXA1 as a potential therapeutic target to improve the efficacy of anti-PD-1/PD-L1 immunotherapy in TNBC.

Keywords Circular RNA · Triple negative breast carcinoma · PD-L1 · GSDMC · Immune escape

Honghong Shen and Boyu Li contributed equally to this work.

Published online: 22 April 2026

Background

Triple-negative breast cancer (TNBC), a distinct subtype of breast cancer characterized by the absence of estrogen receptor (ER), progesterone receptor (PR), and human epidermal growth factor receptor 2 (HER2) expression, remains a major clinical challenge due to the lack of actionable molecular targets for endocrine and anti-HER2 therapies (Wang et al. 2021). Chemotherapy is the mainstay of systemic treatment for TNBC, yet a large proportion of patients develop chemoresistance, leading to disease recurrence, metastasis, and poor clinical outcomes(Ehmsen and Ditzel 2021, Leon-Ferre and Goetz 2024). Notably, TNBC exhibits higher levels of tumor-infiltrating lymphocytes (TILs) and PD-L1 expression compared with other breast cancer subtypes, suggesting that TNBC patients may benefit from immune checkpoint inhibitor (ICI) therapy targeting the PD-1/PD-L1 axis (Leon-Ferre et al. 2024). However, the overall response rate (ORR) of TNBC patients to anti-PD-1/PD-L1 monotherapy remains suboptimal, as demonstrated by the IMpassion 130 trial (Schmid et al. 2020), which is primarily attributed to tumor immune escape. The interaction between PD-L1 on tumor cells and PD-1 on activated $CD8^+$T cells suppresses T cell activation and induces an immunosuppressive TME, which is a key molecular mechanism of TNBC immune evasion (Bréart et al. 2025, Li et al. 2025). Elucidating the upstream regulatory mechanisms of PD-L1 expression and stability in TNBC is therefore urgently required to develop novel strategies for reversing ICI resistance.

Circular RNAs (circRNAs), a class of non-coding RNAs with a covalently closed-loop structure and high stability, have emerged as key regulators of tumor progression and immune regulation (Palcau et al. 2025). Unlike linear RNAs, circRNAs exert biological functions by acting as competing endogenous RNAs (ceRNAs) or directly binding to RNA-binding proteins (RBPs) to regulate the expression of downstream target genes (Liu et al. 2025). Accumulating evidence has shown that circRNAs promote tumor immune escape by modulating PD-L1 expression and impairing $CD8^+$T cell-mediated cytotoxicity (Can et al. 2025, Lan et al. 2025), highlighting their potential as novel biomarkers and therapeutic targets for cancer immunotherapy. However, the functional roles and regulatory mechanisms of circRNAs in TNBC immune escape, especially those modified by epigenetic modifications, remain largely unexplored.

N^6-methyladenosine (m^6A) modification, the most prevalent post-transcriptional modification of RNAs, is dynamically regulated by three core groups of molecules: writers (METTL3, METTL14, WTAP), erasers (FTO, ALKBH5), and readers (YTHDF1/2/3) (Zhang et al. 2025, Murakami et al. 2025). Recent studies have demonstrated that m^6A modification modulates the stability, circularization, and biological functions of circRNAs, and dysregulated m^6A-modified circRNAs contribute to tumor cell proliferation, invasion, and metastasis (Margvelani et al. 2025, Bao et al. 2023). Moreover, m^6A regulators are involved in the regulation of anti-tumor immunity by modulating $CD8^+$T cell infiltration and function (Lin et al. 2024, Wang et al. 2024). Nevertheless, the role of m^6A-modified circRNAs in regulating PD-L1-mediated TNBC immune escape has not been reported to date, and the underlying molecular mechanisms remain unclear.

Gasdermin C (GSDMC), a member of the gasdermin protein family, is a key mediator of pyroptosis and has been implicated in tumor progression and immune regulation (Moini et al. 2025). GSDMC can form membrane pores to trigger pyroptosis, and aberrant GSDMC expression reduces the number and functional capacity of infiltrating $CD8^+$T cells in the TME, thereby promoting tumor immune escape (Moini et al. 2025). However, the upstream regulatory factors of GSDMC in TNBC and its potential crosstalk with the PD-1/PD-L1 immune checkpoint axis have not been elucidated. Additionally, PD-L1 protein stability is tightly regulated by ubiquitination and deubiquitination, and OTUB1, a deubiquitinase, has been shown to stabilize PD-L1 by inhibiting its endoplasmic reticulum-associated degradation (ERAD) (He et al. 2024). However, the upstream molecular mechanisms governing OTUB1 expression and its interaction with GSDMC in TNBC remain unknown.

In this study, we screened TNBC tissues by whole-transcriptome microarray analysis and identified circFOXA1 as an m^6A-modified circRNA negatively correlated with $CD8^+$T cell infiltration. We hypothesized that m^6A-modified circFOXA1 mediates TNBC immune escape by regulating the GSDMC/OTUB1/PD-L1 axis to

inhibit CD8⁺T cell infiltration and function. We further validated this hypothesis through in vitro and in vivo experiments, and clarified the key molecular mechanisms underlying the circFOXA1/GSDMC axis in PD-L1 stabilization and TNBC immune escape. Our findings reveal a novel molecular mechanism of TNBC immune evasion and provide a potential therapeutic target for improving the efficacy of immunotherapy in TNBC patients.

Materials and methods

Human samples

Between January 2012 and December 2017, 55 pairs of primary TNBC tissues and adjacent non-tumor tissues (≥2 cm from the margin) were collected from patients who underwent curative resection at the Second Hospital of Shanxi Medical University. All patients were pathologically diagnosed with TNBC, had not received neoadjuvant therapy, and had no history of other malignancies or autoimmune diseases.

Two pairs of tissues were randomly selected for whole-transcriptome microarray sequencing. Peripheral blood (5 mL) was drawn from each patient preoperatively into EDTA tubes. PBMCs were isolated by centrifugation at 3000 × g for 15 min at 4 °C. All tissue and blood samples were immediately frozen in liquid nitrogen and stored at −80 °C until experimental use.

Cell culture and transfection

Human TNBC cell lines (MDA-MB-231,Hs578T, MDA-MB-468,BT-483) were purchased from the Cell Bank of the Chinese Academy of Sciences (Shanghai) and authenticated by STR profiling. All cells were cultured in DMEM (Gibco) supplemented with 10% FBS (Gibco), maintained in a humidified 37 °C incubator with 5% CO_2, and routinely tested for sterility.

si-circFOXA1#1, si-circFOXA1#2, and si-NC were synthesized by GenePharma. For transient transfection, TNBC cells were transfected with 50 nM siRNA using Lipofectamine 3000 (Invitrogen) per manufacturer's instructions. Transfection efficiency was verified by qRT-PCR at 48 h post-transfection; functional experiments were performed at 48–72 h.

GSDMC-OE plasmid and pcDNA3.1 control (GenScript) were transfected via Lipofectamine 3000. Stable cell lines were selected with 800 μg/mL G418 (Sigma-Aldrich) after 2 weeks of continuous culture.

Preparation and activation of CD8 + T cells

Peripheral blood mononuclear cells (PBMCs) were isolated from the peripheral blood of TNBC patients by density gradient centrifugation using Ficoll-Paque Plus (GE Healthcare, Chicago, IL, USA) at 400 × g for 30 min at room temperature. CD8⁺ T cells were further purified from PBMCs using CD8 MicroBeads UltraPure (Miltenyi Biotec, Bergisch Gladbach, Germany) according to the manufacturer's magnetic-activated cell sorting (MACS) protocol. The purity of isolated CD8⁺ T cells was confirmed to be ≥90% by flow cytometry before subsequent experiments.

For in vitro activation, purified CD8⁺ T cells were cultured in RPMI-1640 medium (Gibco, Thermo Fisher Scientific) supplemented with 10% FBS, 1% penicillin-streptomycin, 50 U/mL recombinant human interleukin-2 (IL-2; Abcam, Cambridge, UK), and stimulated with Dynabeads™ Human T-Activator CD3/CD28 (Gibco, Thermo Fisher Scientific) at a bead-to-cell ratio of 1:1. The cells were cultured for 5–7 days, with half the medium replaced every 2 days, and activated CD8⁺ T cells were collected for co-culture experiments.

T-cell-mediated tumor cell killing experiment

TNBC cells were seeded in 12-well plates at a density of 2×10^5 cells per well and cultured for 24 h to achieve 70–80% confluency. Activated PBMCs (effector cells) were co-cultured with TNBC cells (target cells) at an effector-to-target (E: T) ratio of 3:1 in complete DMEM medium for 48 h. After co-culture, both floating and adherent cells were collected, washed twice with pre-cooled phosphate-buffered saline (PBS; Beyotime), and stained with Annexin V-FITC and propidium iodide (PI) Apoptosis Detection Kit (Vazyme) for 15 min in the dark at room temperature. Tumor cell apoptosis was immediately analyzed by flow cytometry (BD FACSCalibur, BD Biosciences, San Jose, CA, USA), and the data were processed using FlowJo v10.8 software (FlowJo LLC, Ashland, OR, USA). All experiments were performed in triplicate.

Experimental animals and in vivo xenograft models

SPF female C57BL/6 mice (4–5 weeks old, 18–22 g) and PD-L1-deficient C57BL/6 mice were purchased from Beijing Vital River Laboratory Animal Technology. Mice were housed in a specific-pathogen-free facility at Shanxi Medical University under controlled conditions (22 ± 2 °C, 50 ± 10% humidity, 12 h light/dark cycle) with free access to food and water.

TNBC cells (5×10^6 per mouse) were resuspended in 100 µL sterile PBS mixed with Matrigel (1:1, v/v) and subcutaneously injected into the right flank. When tumors reached ~ 50 mm^3, mice were randomly divided into groups ($n = 6$) and intraperitoneally administered CD8 or PD1 monoclonal antibodies, or isotype control IgG2b, every 3 days for 5 doses.

Tumor volume was measured every 3 days ($V = 0.5 \times length \times width^2$). On day 15, mice were euthanized, and mouse weight was monitored throughout the study to assess treatment-related toxicity.

RNase R treatment

Total RNA was extracted from MDA-MB-231 cells using TRIzol™ Reagent (Invitrogen, Thermo Fisher Scientific) in accordance with the manufacturer's protocol, and RNA concentration and purity were determined by a NanoDrop 2000 spectrophotometer (Thermo Fisher Scientific; A260/A280 ratio = 1.8–2.1). For RNase R digestion, 5 µg of total RNA was incubated with 5 U/µg RNase R (Epicentre, Madison, WI, USA) in 1×RNase R reaction buffer at 37 °C for 10 min, and the reaction was terminated by heating at 85 °C for 5s. RNA samples without RNase R digestion were used as the negative control. After digestion, RNA was reverse-transcribed into complementary DNA (cDNA), and the expression levels of circFOXA1 and linear FOXA1 were detected by qRT-PCR to evaluate the resistance of circFOXA1 to RNase R digestion.

qRT-PCR

Total RNA was extracted from TNBC cells and clinical tissues using TRIzol™ Reagent according to the manufacturer's instructions. qRT-PCR was performed on a LightCycler 480 Real-Time PCR System (Roche, Basel, Switzerland) using the SYBR® Premix Ex Taq™ II Kit (TaKaRa). The reaction system (20 µL) consisted of 10 µL of SYBR Premix ExTaq II, 0.4 µL of forward primer (10 µM), 0.4 µL of reverse primer (10 µM), 2 µL of cDNA template, and 7.2 µL of sterile ddH_2O. The relative expression levels of target genes were calculated using the $2^{-}\Delta\Delta Ct$ method, and all experiments were performed in triplicate with three technical replicates per sample.

Actinomycin D assay

MDA-MB-231 cells were seeded in 12-well plates at a density of 2.5×10^5 cells per well and cultured overnight to achieve 70% confluency. Cells were treated with 2 µg/mL actinomycin D (Sigma-Aldrich), a transcription

inhibitor, and an equal volume of dimethyl sulfoxide (DMSO; Sigma-Aldrich) was used as the control. Total RNA was extracted from cells at 0 h, 6 h, 12 h, 18 h, and 24 h after treatment, and the expression level of circFOXA1 (and OTUB1 for subsequent experiments) was detected by qRT-PCR.

Immunofluorescence assay and fluorescence in situ hybridization (FISH)

For FISH to detect circFOXA1 localization, MDA-MB-231 cells were seeded on coverslips, fixed with 4% PFA, permeabilized with 0.5% Triton X-100, and hybridized with Cy3-labeled circFOXA1 probes (Meiji Biotech; see Supplementary Materials) at 37°C overnight. Nuclei were stained with DAPI.

For IF, fixed cells were blocked with 5% BSA, incubated with primary antibodies at 4°C overnight, followed by Alexa Fluor 488/594-conjugated secondary antibodies (Abcam) for 1 h. Cells were counterstained with DAPI and mounted. All experiments were performed in triplicate.

Dual-luciferase assay

The putative OTUB1 promoter region was amplified from human genomic DNA and subcloned into pmirGLO vector (Promega) to construct OTUB1-promoter-pmirGLO plasmid. Cells were co-transfected with 500 ng of this plasmid (or empty pmirGLO as control) and 5 ng pRL-TK (Promega, internal reference) via Lipofectamine 3000. For GSDMC overexpression, cells were co-transfected with GSDMC-OE (or empty vector) and OTUB1-promoter-pmirGLO.

At 48 h post-transfection, luciferase activities were measured using Dual-Luciferase® Assay System (Promega). Relative activity was calculated as firefly/Renilla luciferase ratio.

Flow cytometry

For immune cell infiltration analysis, fresh tumor tissues were minced into 1–2 mm fragments, digested with 0.25% collagenase IV and 0.1% hyaluronidase (Sigma-Aldrich) at 37 °C for 30 min, filtered through a 70 μm strainer (BD Biosciences) to get single-cell suspensions, lysed with red blood cell lysis buffer (Beyotime) for 5 min, and washed with 2% FBS-PBS.

1×10^6 cells/sample were incubated with Fc Block (BD Biosciences) at 4 °C for 10 min, then stained with fluorochrome-conjugated primary antibodies (CD3-APC, CD8-FITC, etc.; BD/eBioscience) in the dark for 30 min (isotype controls for gating). After washing, cells were analyzed by BD FACSCalibur, data processed with FlowJo v10.8. Apoptosis was detected via Annexin V-FITC/PI staining as described.

Quantitative experiment of RNA m6A

The total m^{6}A level in cellular RNA was measured using the EpiQuik™ m^{6}A RNA Methylation Quantification Kit (Colorimetric; Epigentek) following the manufacturer's instructions. Briefly, 200 ng of total RNA was coated onto a 96-well plate at 37 °C for 1 h, followed by blocking with blocking buffer at room temperature for 30 min. The RNA was incubated with m^{6}A-specific capture antibody at room temperature for 1 h and then with detection antibody for 30 min. Enhancer and developer solutions were added sequentially, and the reaction was stopped with stop solution. The absorbance at 450 nm was detected using a Bio-Rad Model 680 microplate reader. A standard curve was generated using serial dilutions of the m^{6}A standard, and the m^{6}A content (percentage of total adenosine) was calculated accordingly. All experiments were performed in triplicate with three technical replicates per sample.

RNA-Pull down assay

Biotin-labeled circFOXA1-specific probes and negative control probes were synthesized by Meiji Biotech (probe sequences see Supplementary Materials). MDA-MB-231 cells were cross-linked with 1% formaldehyde (terminated with 0.125 M glycine), lysed in RIPA buffer (with protease/RNase inhibitors) on ice for 30 min, and sonicated to shear chromatin into 200–500 bp fragments. After centrifugation, 50 µL supernatant was retained as input control.

The rest was incubated with streptavidin dynabeads pre-bound with biotin probes at 30 °C overnight. Bead complexes were washed 5 times, cross-link reversed with proteinase K, RNA extracted by TRIzol™. GSDMC enrichment was detected by qRT-PCR, normalized to input and negative control. All experiments were triplicated.

Methylated RNA immunoprecipitation (MeRIP)

MeRIP assay was conducted to examine m^{6}A modification of circFOXA1 using the Magna MeRIP™ m^{6}A Kit (Millipore) following the manufacturer's instructions. Total RNA (500 µg) isolated from TNBC cells was fragmented into 100–200nt fragments with RNA Fragmentation Reagent (Ambion) at 70 °C for 5 min. A total of 55 ng fragmented RNA was saved as input control. The remainder was incubated with 5 µg anti-m^{6}A antibody (Abcam) or normal rabbit IgG (Millipore, negative control) in IP buffer at 4 °C for 2 h with gentle rotation. Antibody-RNA complexes were captured with Dynabeads® Protein A (Invitrogen) at 4 °C for 1 h. Beads were washed three times with low-salt buffer and once with high-salt buffer. Immunoprecipitated RNA was eluted with m^{6}A elution buffer at 4 °C for 30 min and purified using the RNeasy Mini Kit (Qiagen). circFOXA1 enrichment was quantified by qRT-PCR. Relative m^{6}A levels were calculated as the anti-m^{6}A/IgG ratio normalized to input. All experiments were performed in triplicate.

Bioinformatics Analysis

The circular structure of circFOXA1 was verified by Sanger sequencing. m^{6}A modification sites on circFOXA1 were predicted using the RMBase v2.0 database. The correlation between METTL14 and CD8$^+$ T cell infiltration was analyzed using the TIMER 2.0 database. Co-expression networks of circFOXA1-related mRNAs and GSDMC-related mRNAs were constructed using Cytoscape 3.9.1. Expression and survival analyses were performed using data from The Cancer Genome Atlas (TCGA) Breast Invasive Carcinoma (BRCA) cohort. Genes with $|\log_2(\text{fold change})|>1$ and adjusted $P<0.05$ were considered differentially expressed. Correlation analyses were performed using Spearman's correlation and visualized with corresponding correlation coefficients and P values. All bioinformatics analyses were performed using R software (version 4.2.1) with packages including ggplot2, survival, and glmnet.

Statistical methods

Data are presented as mean ± SD from at least three independent experiments. Statistical analyses were performed using IBM SPSS 25.0 and GraphPad Prism 9.0. The chi-square test was used to assess the correlation between circFOXA1 expression and clinicopathological features in TNBC patients. Survival analysis was conducted using Kaplan-Meier plots with the log-rank test for overall survival (OS) and disease-free survival (DFS). Univariate and multivariate Cox regression models were applied to identify independent prognostic factors. ROC curves and AUC values were used to evaluate the diagnostic performance of circFOXA1. A two-tailed $P<0.05$ was considered statistically significant ($^*P<0.05$, $^{**}P<0.01$).

Results

Identification and characteristic of a novel circRNA, circFOXA1

Based on whole-transcriptome microarray expression profiles of triple-negative breast cancer (TNBC) tissues combined with bioinformatics analysis, our study identified four circRNAs that were negatively correlated with CD8+T cell infiltration (Fig. 1A and B). These candidate circRNAs were further validated by qRT-PCR and RNase R digestion assays. Compared with other candidates, hsa_circ_2796 (designated circFOXA1) was highly expressed in all tested TNBC cell lines (Fig. 1C) and resistant to RNase R treatment (Fig. 1D). Further investigation demonstrated that circFOXA1 exhibited greater stability than linear FOXA1 mRNA following actinomycin D treatment (Fig. 1E). RNA fluorescence in situ hybridization (RNA FISH) confirmed that circFOXA1 was predominantly localized in the nucleus of TNBC cells (Fig. 1F).

Collectively, these results identify circFOXA1 as a highly stable circRNA in TNBC cells.

circFOXA1 is overexpressed in TNBC

Annotation in circBase indicated that circFOXA1 is generated by back-splicing of exons 8 and 22 of linear FOXA1 (Fig. 2A). To explore the clinical significance of circFOXA1 expression in TNBC, we explored the clinical significance of circFOXA1 in the progression of triple-negative breast cancer (TNBC). First, qRT-PCR results demonstrated that circFOXA1 expression was significantly upregulated in TNBC tissues compared with adjacent non-tumor tissues (Fig. 2B). Second, receiver operating characteristic (ROC) curve analysis was performed to evaluate the sensitivity and specificity of circFOXA1, which revealed that circFOXA1 could serve as a novel diagnostic biomarker for TNBC (Fig. 2C). Finally, Kaplan-Meier curve analysis and Cox regression analysis were employed to assess the prognostic significance of circFOXA1. Survival analysis showed that patients with high circFOXA1 expression had significantly shorter overall survival (Fig. 2D). Additionally, univariate and

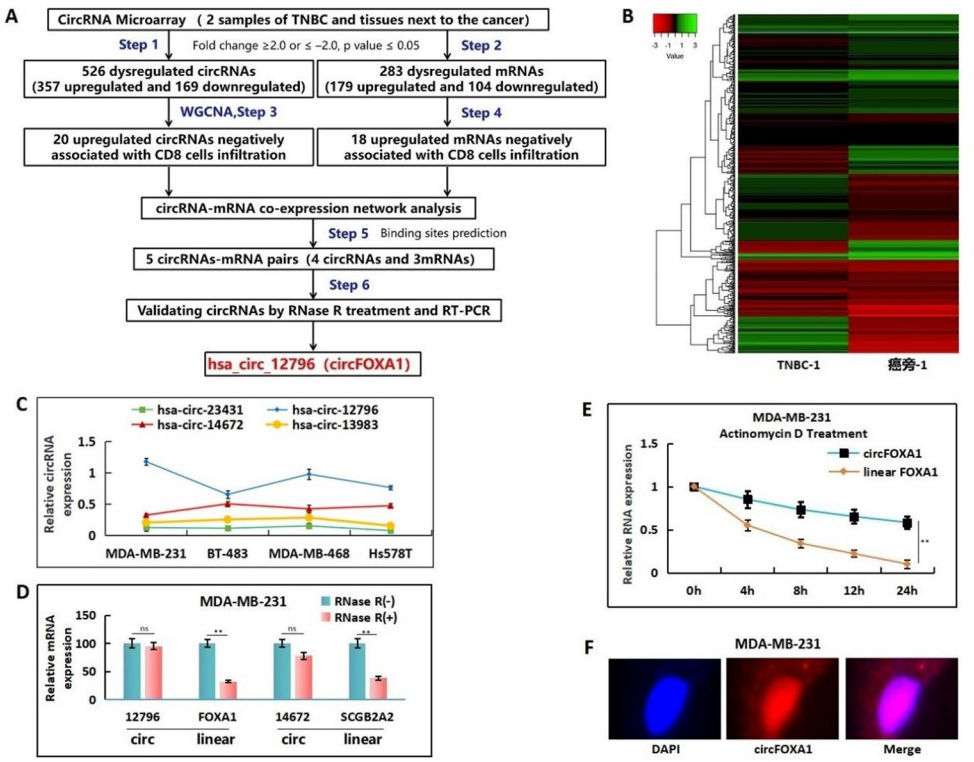

Fig. 1 Identification and characterization of circFOXA1 in TNBC. (A) Flowchart of screening circFOXA1 based on sequencing results combined with bioinformatics. (B) Cluster analysis of the expression profiles of circRNAs microarrays in TNBC tissues and adjacent tissues. (C) qRT-PCR was used to detect the expression of circRNAs in TNBC cell lines. (D) qRT-PCR was used to detect the expression of circFOXA1 in TNBC cells after Rnase R digestion. (E) The stability of circFOXA1 after actinomycin treatment was detected by qRT-PCR. (F) RNA FISH verified the localization of circFOXA1 in MDA-MB-231 cells, Magnification:200×. $^{**}P<0.01$

Table 1 abc

Clinicopathological factors	N	N (%)		P value
		circFOXA1low	circFOXA1high	
Total	55	21 （38.2	34 （61.8	
Aage				0.218
≤50	20	8 （40.0）	12 （60.0）	
＞50	35	13 （37.1）	22 （62.9）	
Tumor size(cm)				0.095
≤2	18	8 （44.4）	10 （55.6）	
＞2；≤5	20	9 （45.0）	11 （55.0）	
＞5	17	4 （23.5）	13 （76.5）	
Grade				0.035*
G1-G2	39	18 （46.2）	21 （53.8）	
G3	16	3 （18.7）	13 （81.3）	
Stage				0.066
I	22	13 （59.1）	9 （40.9）	
II	28	6 （21.4）	22 （78.6）	
III	5	2 （40.0）	3 （60.0）	
Lymphovascular invasion				0.126
No	43	17 （39.5）	26 （60.5）	
Yes	12	4 （33.3）	8 （66.7）	
Ki67				0.019*
＜20%	13	8 （61.5）	5 （38.5）	
≥20%	42	13 （31.0）	29 （69.0）	

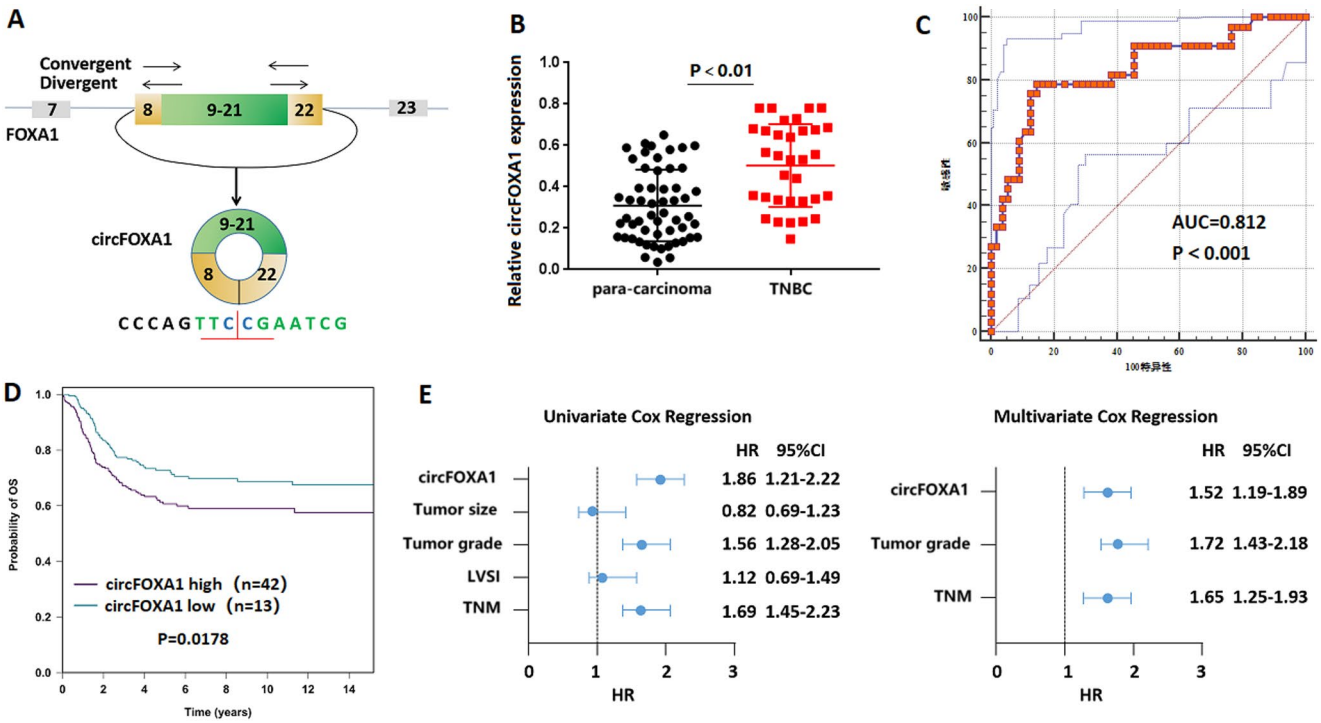

Fig. 2 Clinical significance and prognostic value of circFOXA1 in TNBC.(A) Sanger sequencing confirmed the circular structure of circFOXA1. (B) The expression of circFOXA1 in tissues was detected by qRT-PCR. (C) The ROC curve was used to evaluate the sensitivity and specificity of circFOXA1 detection. (D) Kaplan-Meier curve was used to evaluate the relationship between circFOXA1 levels and patient OS. (E) Cox regression analysis showed that circFOXA1 was an independent prognostic biomarker in TNBC

multivariate Cox regression analyses suggested that high circFOXA1 expression is an independent prognostic indicator for TNBC (Fig. 2E).

Subsequently, we analyzed the correlation between circFOXA1 expression levels and clinicopathological characteristics of 55 TNBC patients. As shown in Table 1, according to the median expression level of circFOXA1, the patients were divided into two groups: the circFOXA1 group ($n=21$, 38.2%) and the circFOXA1 group ($n=34$, 61.8%). The results showed that circFOXA1 expression was significantly associated with tumor grade and Ki67 proliferation index (both $P<0.05$). These findings suggest that high circFOXA1 expression is closely related to more aggressive tumor phenotypes in TNBC patients, implying that circFOXA1 may serve as a potential indicator of tumor progression.

circFOXA1 attenuates CD8 + T cell-mediated antitumor immunity

To verify whether circFOXA1 participates in the immune regulation of triple-negative breast cancer (TNBC), we performed a T cell-mediated cytotoxicity assay. TNBC cells were first co-cultured with peripheral blood mononuclear cells (PBMCs). After silencing circFOXA1 expression, flow cytometry demonstrated that PBMC-mediated cytotoxicity (tumor cell apoptosis) was significantly enhanced (Fig. 3A).

To further investigate whether circFOXA1 mediates the immunosuppressive effects exerted by tumor cells on peripheral blood mononuclear cells (PBMCs), immunological functional assays were performed. As illustrated in Fig. 3B and C, knockdown of circFOXA1 significantly relieved tumor cell-induced immunosuppression, as evidenced by elevated expression of perforin and granzyme B (GzmB), as well as increased secretion of IFN-γ and TNF-α in co-cultured PBMCs. In contrast, ectopic overexpression of circFOXA1 suppressed the expression and secretion of these anti-tumor immune effectors. Furthermore, PBMCs co-cultured with circFOXA1-silenced tumor cells displayed enhanced Ki-67 positivity and reduced TUNEL-positive apoptotic rates, whereas circFOXA1 overexpression markedly restrained PBMC proliferation and promoted apoptosis (Fig. 3D and E). To determine whether circFOXA1-induced immunosuppression is dependent on CD8 + T cells, circFOXA1-overexpressing TNBC cells were inoculated into immunocompetent C57BL/6 mice. Administration of CD8 neutralizing antibody (CD8 mAb) significantly promoted tumor growth (Fig. 3F). Flow cytometry analysis showed that, compared with the IgG2b control group, circFOXA1 overexpression reduced tumor-infiltrating CD8 + T cells (Fig. 3G), as well as the proportions of IFN-γ+ (Fig. 3H), TNF-α+ (Fig. 3I), GzmB+ (Fig. 3J), and perforin+ (Fig. 3K) CD8 + T cells. These data demonstrate that the immunosuppressive function of circFOXA1 relies on the inhibition of CD8 + T cell activity and infiltration.

Elevated circFOXA1 expression in TNBC is due to m6A RNA methylation

m6A methylation is known to be involved in tumor immune escape. To investigate whether circFOXA1 is regulated by m6A modification, we first predicted potential m6A modification sites in circFOXA1 using RMBase 2.0. Bioinformatics prediction results confirmed the presence of m6A modification sites in circFOXA1 (Fig. 4A). Furthermore, methylated RNA immunoprecipitation (MeRIP) assays showed that TNBC cells with high circFOXA1 expression exhibited higher enrichment of m6A modification compared to those with low circFOXA1 expression (Fig. 4B). Aberrant expression of m6A writers has been reported to contribute to malignant tumor progression. To explore whether m6A modification regulates the expression and function of circFOXA1, we separately silenced the m6A writer genes METTL3, METTL14, and WTAP. The results showed that only METTL14 knockdown significantly decreased circFOXA1 expression (Fig. 4C). Consistent with this, MeRIP-qPCR assays demonstrated reduced m6A modification enrichment in TNBC cells after METTL14 silencing (Fig. 4D). RIP assays further validated the direct interaction between circFOXA1 and METTL14 (Fig. 4E). Notably, treatment with MAO-circFOXA1 abolished the regulatory effect of METTL14 on circFOXA1 expression (Fig. 4F). TIMER 2.0 bioinformatics analysis revealed that METTL14 negatively regulated CD8 + T cell infiltration (Fig. 4G). In addition, literature reports and our experimental results showed that silencing YTHDF2 (an m6A reader) in TNBC cells

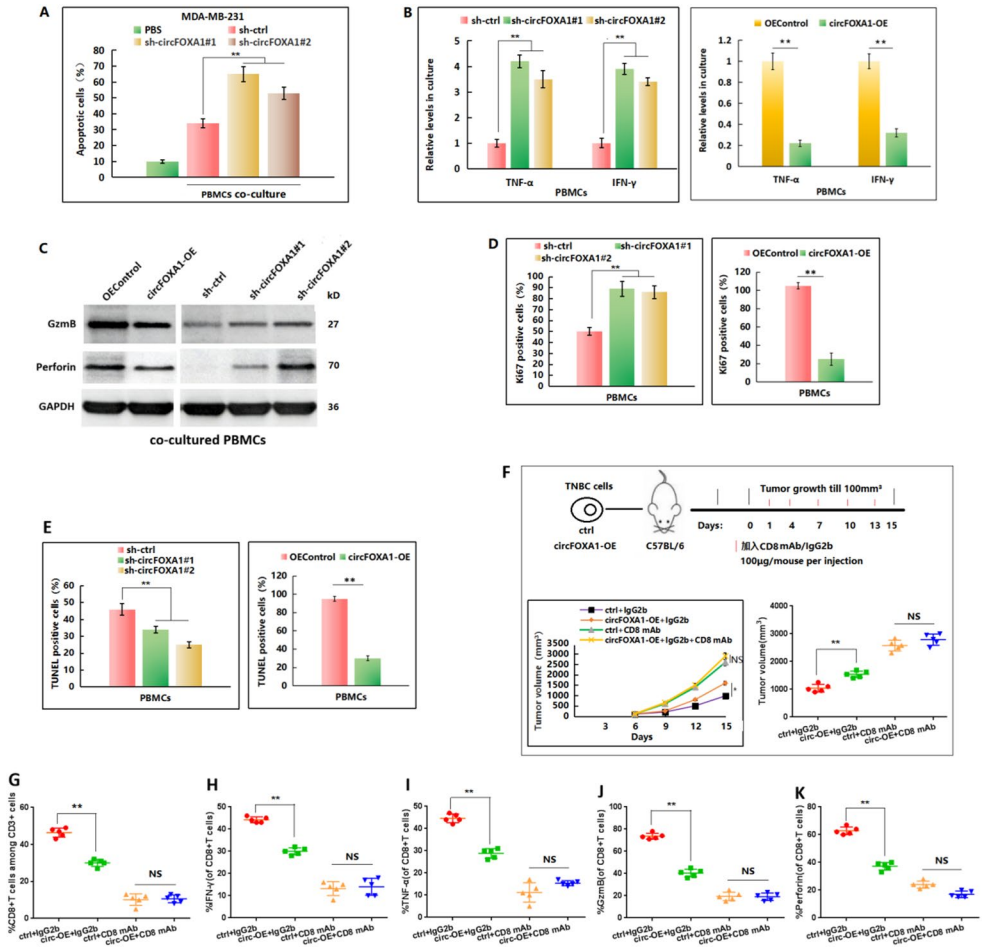

Fig. 3 Silencing circFOXA1 enhances anti-tumor immunity in TNBC. Silencing the expression of circFOXA1 in TNBC cells, (A) Flow cytometry (FACS) analysis of the ability of PBMCs to promote tumor cell apoptosis. (B) ELISA was used to analyze the secretion levels of immune effector factors IFN-γ and TNF-α. (C) Western-blot was used to detect the expressions of Perforin and GzmB. (D) Ki67-positive cell count was used to detect the proliferation ability of PBMCs. (E) The apoptotic ability of PBMCs was verified by the TUNEL method. (F) Schematic diagram of the grouping and treatment plan of the mouse model, with tumor volume measured every 3 days. Flow cytometry was used to detect the infiltration quantities of (G) CD8 + T cells, (H) IFN-γ + CD8 + T cells, (I) TNF-α + CD8 + T cells, (J) GzmB+ CD8 + T cells and (K) perforin+ CD8 + T cells. $^{**}P < 0.01$, $^{*}P < 0.05$

significantly reduced circFOXA1 expression, while the expression of linear FOXA1 mRNA remained unchanged (Fig. 4H). RIP assays validated that circFOXA1 serves as a bona fide binding partner of YTHDF2 (Fig. 4I). Furthermore, m6A inhibition mediated by MAO-circFOXA1 nearly completely abrogated the positive regulatory effect of YTHDF2 on circFOXA1 expression (Fig. 4J).

Collectively, these results indicate that the m6A writer METTL14 can regulate the m6A modification of circFOXA1, and the m6A reader YTHDF2 can promote circFOXA1 circularization.

circFOXA1 suppresses antitumor immunity in TNBC by elevating GSDMC expression

A total of 44 mRNAs co-expressed with circIGF2BP3 were identified from the GSE186102 and GSE95700 datasets (Fig. 5A). Among these co-expressed mRNAs, GSDMC, CXCR2, and TP53 were further selected as candidate target mRNAs of circFOXA1. Bioinformatics analysis revealed a negative correlation between GSDMC expression and CD8 + T cell infiltration (Fig. 5B). Survival analysis based on The Cancer Genome Atlas (TCGA)

A

Potential m6A sites predicted by RMbase 2.0

ModChr	Mod Start	Mod End	Mod ID	Motif score	Support Num	Region
chr10	15628789	15628790	m6A_site_320190	217.79	1	cds,exon,utr3
chr10	15628796	15628797	m6A_site_320191	309.77	1	exon,utr3,cds

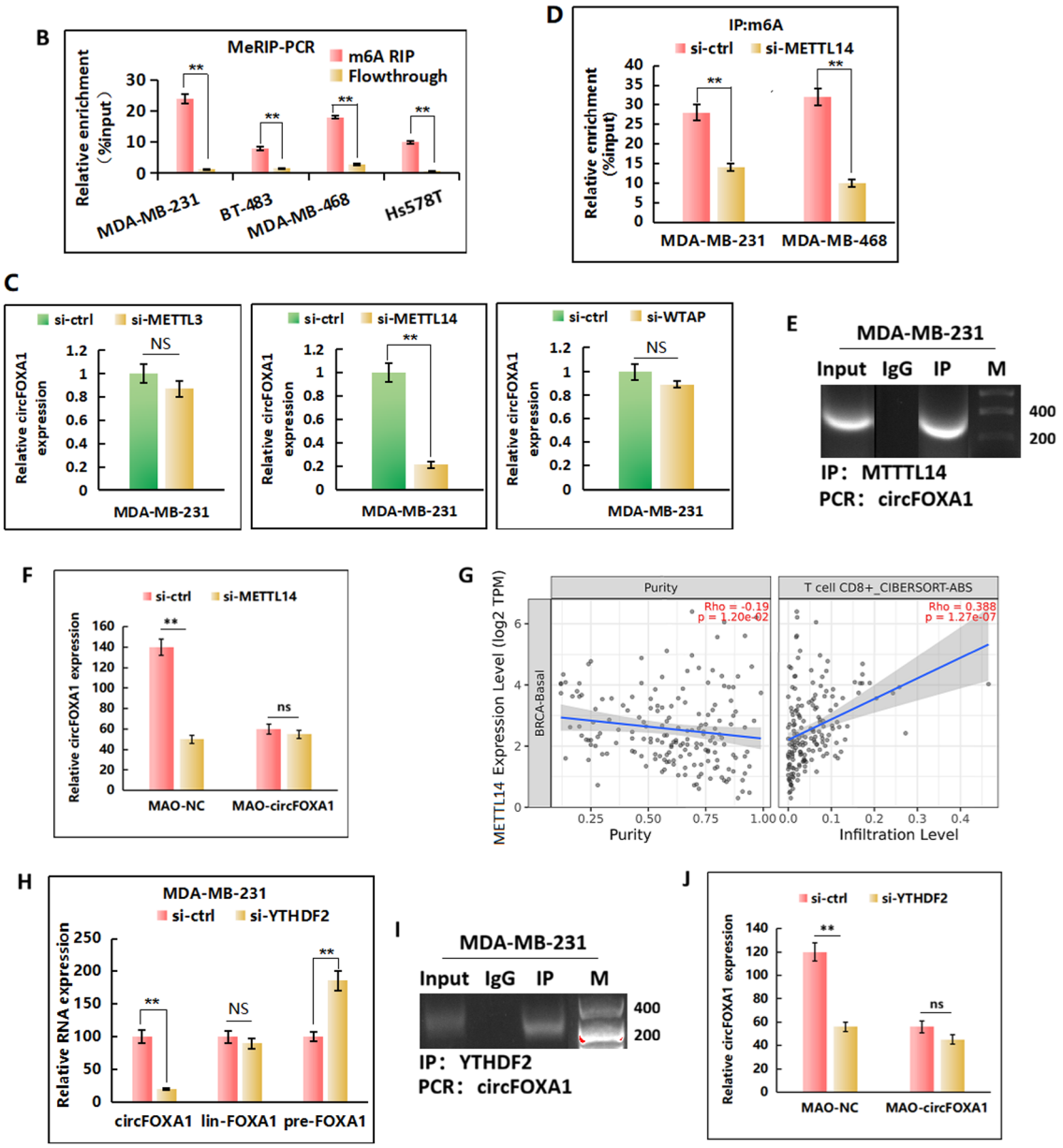

Fig. 4 m6A modification regulates circFOXA1 expression and immune infiltration in TNBC. (A) The m6A modification site of circFOXA1 waspredicted by RMBase2.0. (B) MeRIP analysis of m6A modification enrichment of circFOXA1 in TNBC cells. (C) After knockdown of METTL14/3 and WTAP, qRT-PCR was used to detect the expression of circFOXA1; (D) MeRIP analysis showed that the m6A modification of circFOXA1 was enriched after knockdown of METTL14. (E) METTL14 IP assay to detect circFOXA1 in MDA-MB-231 cells. (F)The relative expression of circFOXA1 in si-METTL14 or si-ctrl MDA-MB-231 cells after treatment with MAO-circFOXA1 or MAO-NC, as detected by qRT-PCR. (G) TIMER 2.0 was used to analyze the correlation between METTL14 and CD8+T cell infiltration. (H) The expression of circFOXA1 and linear FOXA1 RNA was detected by qRT-PCR after YTHDF2 knockdown. (I) YTHDF2 assay to detect circFOXA1 in MDA-MB-231 cells. (J)The relative expression of circFOXA1 in si-YTHDF2 or si-ctrl MDA-MB-231 cells after treatment with MAO-circFOXA1 or MAO-NC, as detected by qRT-PCR. Data represent the mean±SD. $^{**}P<0.01$

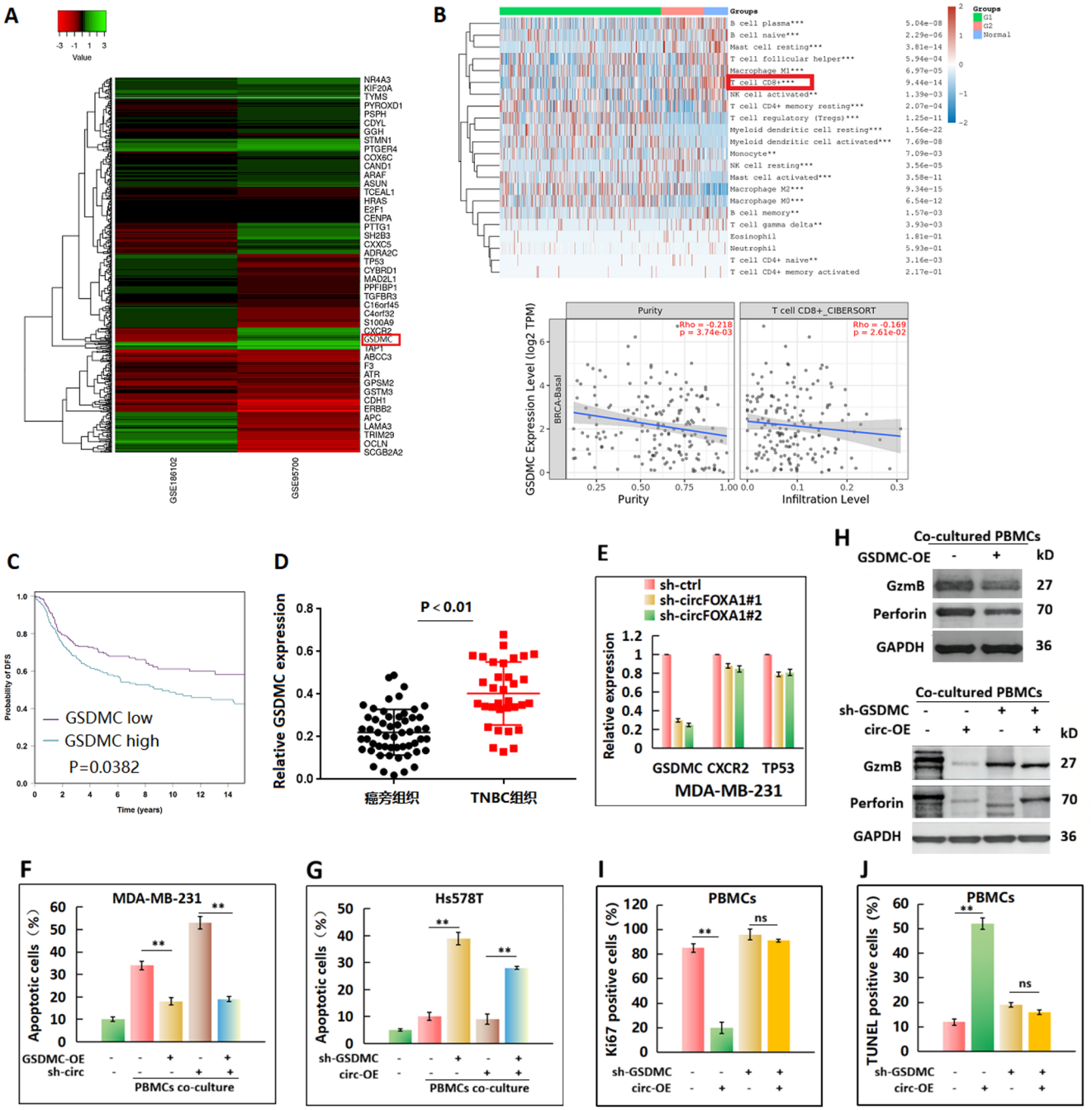

Fig. 5 circFOXA1 regulates GSDMC expression and anti-tumor immunity in TNBC. (A) Cytoscape analysis of the co-expression network of circFOXA1 and its related mRNAs. (B) Bioinformatics analysis of the relationship between GSDMC and CD8+T cell infiltration. (C) TCGA database analysis of the relationship between GSDMC expression and patient prognosis. (D) qRT-PCR detection of GSDMC expression levels in TNBC tissues and adjacent tissues. (E) Silencing the expression of circFOXA1 in TNBC, the relative expression of GSDMC, CXCR2 and TP53 was detected by qRT-PCR. (F, G) FACS analysis of the ability of PBMC-mediated tumor cell apoptosis. (H) The protein levels of Perforin and GzmB in activated PBMCs after coculturing with the indicated TNBC cells were detected by Western Blot. I-J Ki-67 (I) and TUNEL (J) staining of PBMCs after coculturing with the indicated TNBC cells. $^{**}P<0.01$

database demonstrated that higher GSDMC expression was significantly associated with poorer disease-free survival (DFS) in patients (Fig. 5C). Importantly, we observed that GSDMC was highly expressed in TNBC tissue samples compared with their adjacent non-tumor tissues (Fig. 5D).

Quantitative real-time polymerase chain reaction (qRT-PCR) results indicated that silencing circFOXA1 expression remarkably reduced GSDMC mRNA levels (Fig. 5E). Although circFOXA1 expression was correlated with CXCR2 and TP53 expression, no significant changes in the relative expression of CXCR2 and TP53 were detected after circFOXA1 silencing (Fig. 5E). To further explore whether the immunosuppressive effect of circFOXA1 is mediated by GSDMC, we constructed GSDMC-overexpressing (GSDMC-OE) and circFOXA1-silenced (sh-circFOXA1) cell lines, which were then co-cultured with peripheral blood mononuclear cells (PBMCs).

Functional validation using an in vitro T cell–mediated cytotoxicity assay demonstrated that silencing GSDMC significantly sensitized TNBC cells to PBMC-dependent cytolysis and elevated the expression of cytotoxicity-related effector molecules in co-cultured PBMCs. Conversely, enforced overexpression of GSDMC elicited opposing effects (Fig. 5F–H). Notably, GSDMC overexpression strongly augmented the immunosuppressive properties of TNBC cells, whereas GSDMC knockdown effectively reversed the immunosuppressive phenotype induced by circFOXA1 (Fig. 5I–J).

Collectively, these results suggest that circFOXA1 may impair immune cell-mediated tumor cell killing by promoting GSDMC expression and inhibiting CD8+T cell infiltration, thereby facilitating immune escape in TNBC.

GSDMC mediates PD-L1 deubiquitination through OTUB1 to stabilize PD-L1 expression

To identify potential regulators of PD-L1 in TNBC, we first constructed a protein-protein interaction (PPI) network centered on GSDMC using the STRING database, which revealed interactions between GSDMC and multiple immune-related molecules, including PD-L1 and OTUB1 (Fig. 6A). We next investigated whether circFOXA1 modulates GSDMC transcription. Luciferase reporter assays demonstrated that knockdown of circFOXA1 significantly decreased, while overexpression of circFOXA1 increased, the luciferase activity of the GSDMC promoter in both MDA-MB-231 and Hs578T TNBC cell lines (Fig. 6B, $P<0.01$). Correlation analysis of TNBC patient transcriptomic data further confirmed a positive correlation between GSDMC expression and PD-L1 or OTUB1 expression (Fig. 6C). Functional studies revealed that GSDMC regulates PD-L1 expression through OTUB1. In MDA-MB-231 cells, overexpression of GSDMC (GSDMC-OE) increased PD-L1 protein levels, and this effect was abolished by simultaneous knockdown of OTUB1 (Fig. 6D). Conversely, knockdown of OTUB1 decreased, while overexpression of OTUB1 increased, the protein levels of both OTUB1 and PD-L1 in Hs578T and MDA-MB-231 cells (Fig. 6E). To explore the mechanism by which GSDMC regulates OTUB1, we performed luciferase reporter assays and found that GSDMC overexpression had no significant effect on OTUB1 promoter activity (Fig. 6F). Instead, mRNA stability analysis using actinomycin D showed that GSDMC overexpression significantly prolonged the half-life of OTUB1 mRNA in MDA-MB-231 cells (Fig. 6G, $P<0.01$). To test whether GSDMC also regulates OTUB1 expression in this manner, we first analyzed GSDMC-bound RNA by RIP. The results showed that GSDMC could interact with OTUB1 mRNA (Fig. 6H). Clinical relevance of the GSDMC-OTUB1 axis was evaluated using Kaplan-Meier survival analysis, which revealed that high OTUB1 expression was significantly associated with poor overall survival in TNBC patients (Fig. 6I, $P=0.0426$). In vivo tumor growth assays demonstrated that knockout of PD-L1 (sgCD274) suppressed tumor growth, and overexpression of GSDMC partially reversed this effect (Fig. 6J, $P<0.05$). Furthermore, combined treatment with anti-PD-1 monoclonal antibody (mAb) and GSDMC knockdown (shGSDMC) resulted in a more pronounced inhibition of tumor growth compared to either treatment alone (Fig. 6K, $P<0.01$). IHC staining showed that GSDMC expression was positively correlated with PD-L1 expression (Fig. 6L, $P<0.01$).

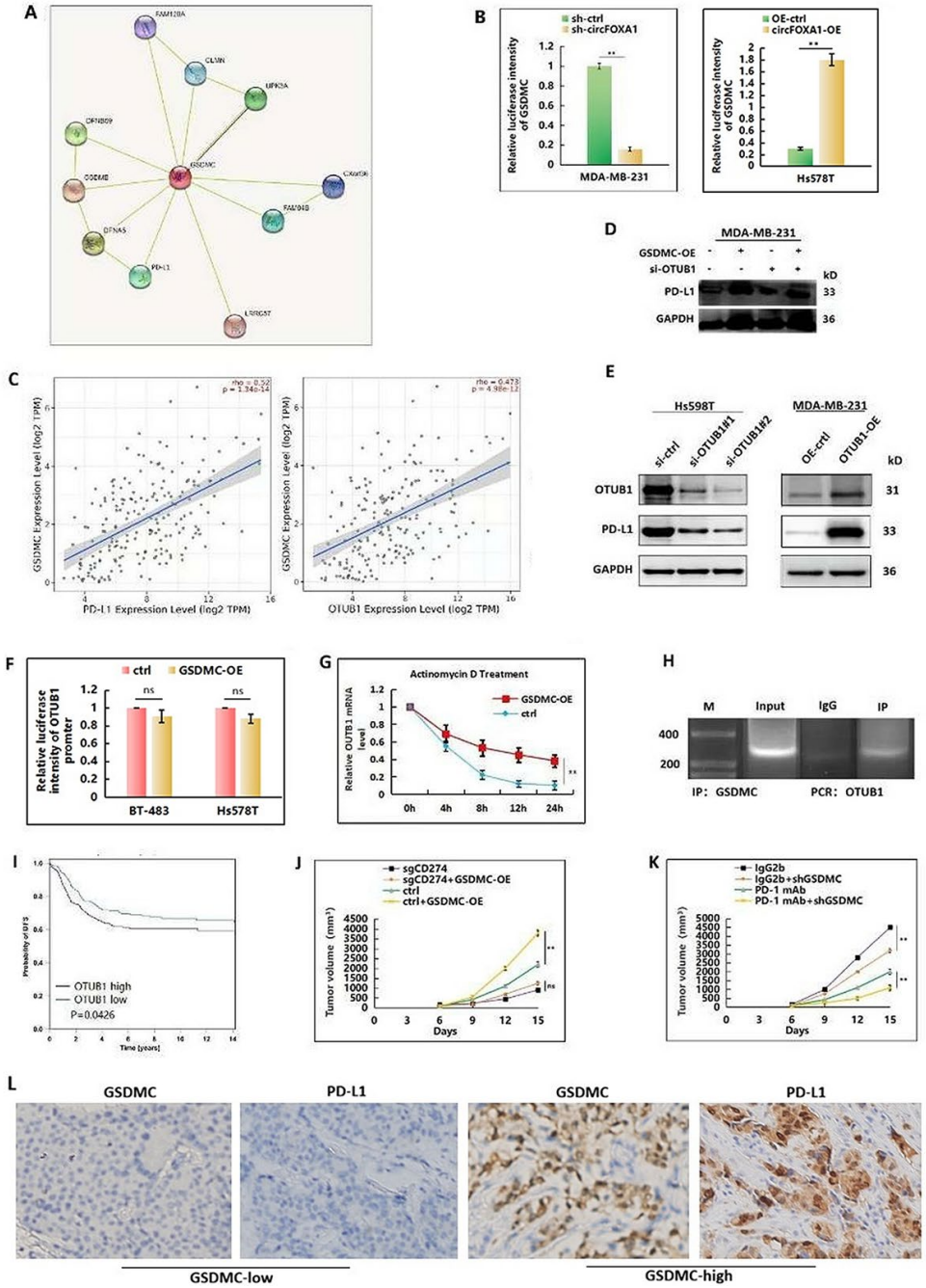

Fig. 6 circFOXA1 regulates PD-L1 expression via GSDMC-OTUB1 axis in TNBC. (A) Bioinformatics analysis GSDMC mRNA co-expressed network. After overexpression of GSDMC in TNBC. (B) The relative luciferase activity of the GSDMC–3'UTR reporter in circFOXA1-silenced (left) and circFOXA1-overexpressing (right) TNBC cells. (C)Correlation analysis between GSDMC and PD-L1 (left) or OTUB1 (right) expression in TNBC patient samples (log_2 TPM). Spearman's correlation coefficient (rho) and p-values are indicated. (D) TNBC cells were co-transfected with GSDMC-OE and si-OTUB1, and the expression of PD-L1 was detected by Western-Blot. (E) Western Blot analysis of OTUB1 and PD-L1 protein levels in TNBC cells with OTUB1 knockdown(left) or overexpression(right). GAPDH was used as a loading control.(F)The luciferase activity of OTUB1 promoter after overexpressing GSDMC was detected by dual luciferase reporter gene. (G) TNBC cells overexpressing GSDMC were treated with actinomycin D, and OTUB1 expression was analyzed by qRT-PCR. (H) GSDMC IP assay to detect OTUB1 mRNA in MDA-MB-231 cells. (I) TCGA analysis of the relationship between OTUB1 expression and patient prognosis. (J) C57BL/6 mice were inoculated with 10^6 CTRL, CTRL+GSDMC-OE, sgCD274 or sgCD274+GSDMC-OE MDA-MB-231 cells, and the tumor volume was measured at the indicated time points.(K)C57BL/6 mice were inoculated with 10^6 shControl or sh-GSDMC MDA-MB-231 cells and received PD-1 mAb treatment or IgG2b control at the. (L) Representative images of IHC staining of GSDMC and PD-L1 in TNBC samples. Magnification: 200×. $^{**}P<0.01$

Collectively, these findings establish that circFOXA1 transcriptionally activates GSDMC, which in turn upregulates OTUB1 expression to stabilize PD-L1, thereby promoting immune evasion in TNBC. Targeting this axis may represent a promising therapeutic strategy to enhance the efficacy of anti-PD-1 immunotherapy in TNBC.

Discussion

A large number of studies have demonstrated that circular RNAs (circRNAs) regulate tumor cell proliferation, invasion, and migration (Shi et al. 2024), yet their immunological functions remain largely underexplored. Using whole-transcriptome microarray profiling of triple-negative breast cancer (TNBC) tissues combined with bioinformatics analysis, our study identified circFOXA1 as a candidate circRNA negatively correlated with CD8+T cell infiltration. Notably, recent work has established circRNA-based signatures for predicting immunotherapeutic response, underscoring the clinical relevance of circRNAs in personalized cancer immunotherapy (Wei et al. 2025). Accordingly, the role of circFOXA1 in TNBC immune escape merits in-depth investigation.

In the present study, circFOXA1 was significantly upregulated in TNBC tissues and exhibited favorable sensitivity and specificity as a novel diagnostic biomarker, consistent with a previous report (Xu et al. 2024). Functionally, knockdown of circFOXA1 enhanced the immune-mediated killing of tumor cells by peripheral blood mononuclear cells (PBMCs). In C57BL/6 mouse models, administration of CD8 monoclonal antibody (CD8mAb) markedly promoted tumor growth. These findings indicate that circFOXA1 may attenuate CD8+T cell infiltration, thereby impairing anti-tumor immune surveillance and facilitating TNBC immune escape. Thus, circFOXA1 represents a potential therapeutic target for improving the efficacy of TNBC immunotherapy, whose detailed mechanism will be further explored in this study.

N6-methyladenosine (m6A) modification contributes to tumor immune escape through diverse regulatory mechanisms (Chen et al. 2025, Xiao et al. 2024). To determine whether circFOXA1 is modulated by m6A, we performed bioinformatics analysis, which predicted m6A modification sites within circFOXA1. Consistently, m6A enrichment was more prominent in TNBC cells with high circFOXA1 expression, a regulatory axis rarely reported in the current literature.

Recent studies have shown that selective enrichment of the m6A regulators METTL14 and YTHDF2 modulates the balance between cytotoxic and dysfunctional CD8+T cells (Zhang et al. 2023). To clarify whether m6A modification controls circFOXA1 expression and function, we knocked down major m6A "writers" (METTL3, METTL14, and WTAP) individually. Only METTL14 knockdown reduced circFOXA1 expression. TIMER2.0 analysis further revealed a negative correlation between METTL14 and CD8+T cell infiltration. Moreover, YTHDF2 knockdown in TNBC cells significantly decreased circFOXA1 expression without altering linear FOXA1 mRNA levels. These results suggest that METTL14 mediates m6A modification of circFOXA1, while YTHDF2 promotes its circularization. The precise molecular cascade through which m6A modification governs TNBC immune escape requires further validation.

Compared with linear host gene exons, circRNAs are highly enriched in RNA-binding protein (RBP) binding sites, and circRNA–RBP interactions play critical roles in tumorigenesis and progression (Liang et al. 2025). Using bioinformatics screening, we identified GSDMC as one of the mRNAs co-expressed with circFOXA1. GSDMC was negatively correlated with CD8+T cell infiltration, and its high expression was associated with inferior disease-free survival (DFS) in TNBC patients. Notably, GSDMC exhibited the most significant differential expression in TNBC tissues. Previous studies reported that circRNA knockdown upregulates pyroptosis-related proteins and induces tumor cell pyroptosis (Zhang et al. 2025, Du et al. 2025). To test whether the immunosuppressive function of circFOXA1 is mediated by GSDMC, we established cell lines co-expressing sh-circFOXA1 and GSDMC-overexpression vectors. In vitro T cell-mediated cytotoxicity assays demonstrated that GSDMC overexpression reversed the enhanced anti-tumor immune response induced by circFOXA1 silencing. These data imply that circFOXA1 modulates CD8+T cell infiltration via GSDMC, thereby promoting TNBC immune escape. Given recent reports that m6A-modified circRNAs regulate macrophage-mediated tumor cell

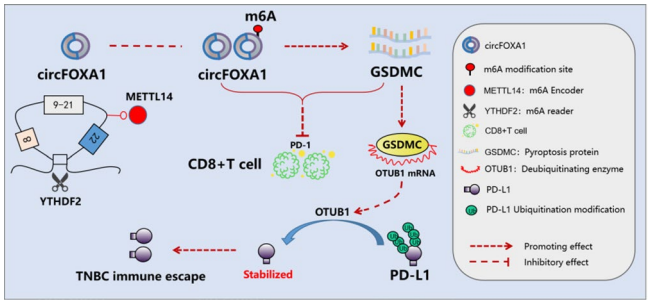

Fig. 7 The hypothesis of m6A modification circFOXA1 mediates TNBC immune escape The m6A modified encoder METTL14 mediates the methylation of circFOXA1, and the reader YTHDF2 can promote the circularization of circFOXA1. circFOXA1 inhibits CD8+T cell infiltration by promoting the expression of GSDMC. At the same time, GSDMC mediates PD-L1 deubiquitination through OTUB1 (deubiquitinating enzyme) to stabilize PD-L1 expression, eventually leading to TNBC immune escape

pyroptosis (Guo et al. 2020), the detailed mechanism underlying circFOXA1/GSDMC-driven immune escape in an m6A-dependent manner warrants further investigation.

Emerging evidence indicates crosstalk between the pyroptosis pathway and immune checkpoints, particularly PD-1/PD-L1 (Tan et al. 2026). Combinatorial strategies targeting pyroptosis regulators and PD-1 monoclonal antibodies have also been proposed for cancer treatment (Zhou et al. 2024). To examine whether circFOXA1/GSDMC-mediated immune escape involves PD-L1 regulation, we evaluated PD-L1 expression in TNBC cells. GSDMC overexpression robustly increased PD-L1 protein levels without affecting PD-L1 mRNA abundance, indicating post-transcriptional regulation.

We next explored the mechanism by which GSDMC stabilizes PD-L1 via deubiquitination. Although CSN5, USP22, and OTUB1 have been reported to deubiquitinate PD-L1 (Hu et al. 2021, Zhu et al. 2021), our data revealed that only OTUB1 knockdown abrogated GSDMC-mediated PD-L1 upregulation. OTUB1, a deubiquitinase, maintains low ubiquitination of newly synthesized PD-L1 and prevents its endoplasmic reticulum-associated degradation (ERAD), leading to sustained PD-L1 overexpression in tumors (Zhang et al. 2025). Additionally, OTUB1 modulates CD8+T cell and NK cell reprogramming and activation, representing a promising target for cancer immunotherapy (Liao et al. 2022). TCGA database analysis showed a positive correlation between GSDMC and OTUB1 mRNA expression in TNBC. Survival analysis further linked high OTUB1 expression to poor DFS. Mechanistically, GSDMC enhanced OTUB1 mRNA stability and upregulated OTUB1 expression at the post-transcriptional level. Collectively, these findings support that GSDMC promotes PD-L1 deubiquitination and stabilization through OTUB1. The circFOXA1/GSDMC/OTUB1/PD-L1 axis thus contributes to TNBC immune evasion (Fig. 7).

Several limitations in the present study should be acknowledged. First, although we proposed that GSDMC promotes PD-L1 stability through upregulating OTUB1, in vivo ubiquitination assays (IP-Ub) were not performed to directly validate the deubiquitination event. Further biochemical studies are required to confirm whether GSDMC facilitates OTUB1-mediated PD-L1 deubiquitination and protein stabilization. Second, the regulatory role of m^{6}A modification on circFOXA1 was preliminarily explored, yet m^{6}A site mutation and corresponding rescue experiments were not conducted due to technical challenges in vector construction and circRNA structural complexity. Future studies with site-directed mutagenesis and functional rescue assays will help clarify the precise m^{6}A-dependent mechanism underlying circFOXA1 regulation.

Conclusion

Collectively, our findings demonstrate that the circFOXA1/GSDMC axis-mediated immune escape in TNBC may be regulated via PD-L1. Mechanistically, GSDMC enhances PD-L1 protein stability through OTUB1-dependent deubiquitination. By delineating the regulatory network underlying immune escape in TNBC and identifying novel therapeutic targets, our study aims to restore T-cell infiltration and anti-tumor immunity within the tumor microenvironment, thereby providing a theoretical foundation for the development of precise immunotherapeutic strategies for TNBC patients.

Acknowledgements We gratefully acknowledge contributions from the TCGA and GEO databases.

Author contributions Honghong Shen, Changqing Zhao and Chen Wang designed the study. Data analysis, figure preparation, manuscript drafting and most of the experiments were performed by Boyu Li and Xiaoqian Wen. Honghong Shen assisted with some of the experiments. All authors read and approved the final manuscript.

Funding This study was supported by the National Natural Science Foundation of China (No.82003204) and Shanxi Science Foundation (No.202303021221202).

Data availability No datasets were generated or analysed during the current study.

Declarations

Conflict of interest The authors declare no conflict of interest.

Ethical approval This study was approved by the Second Clinical Medical College, Shanxi Medical University, China and has been performed in accordance with the ethical standardslaid down in the 1964 Helsinki declaration and its later amendments.

Informed consent Informed consent was obtained from all individual patients enrolled in the study.

References

Bao Y, Zhai J, Chen H et al (2023) Targeting m6A reader YTHDF1 augments antitumour immunity and boosts anti-PD-1 efficacy in colorectal cancer. Gut 72(8):1497–1509

Bréart B, Williams K, Krimm S et al (2025) IL-27 elicits a cytotoxic CD8 + T cell program to enforce tumour control. Nature 639(8055):746–753

Can C, Yang X, Jia H et al (2025) Exosomal circ_0006896 promotes AML progression via interaction with HDAC1 and restriction of antitumor immunity. Mol Cancer 24(1):4

Chen Z, Zeng C, Yang L et al (2025) YTHDF2 promotes ATP synthesis and immune evasion in B cell malignancies. Cell 188(2):331-351.e30

Du K, Zhang X, Qin Y et al (2025) MAP3K13-232aa encoded by circMAP3K13 enhances cisplatin-induced pyroptosis by directly binding to IKKα in gastric adenocarcinoma. Cell Death Dis 16(1):667

Ehmsen S, Ditzel HJ (2021) Signaling pathways essential for triple-negative breast cancer stem-like cells. Stem Cells 39(2):133–143

Guo M, Yan R, Ji Q et al (2020) IFN regulatory factor-1 induced macrophage pyroptosis by modulating m6A modification of circ_0029589 in patients with acute coronary syndrome. Int Immunopharmacol 86:106800
He C, Xing X, Chen HY et al (2024) UFL1 ablation in T cells suppresses PD-1 UFMylation to enhance anti-tumor immunity. Mol Cell 84(6):1120-1138e.e8
Hu X, Wang J, Chu M et al (2021) Emerging role of ubiquitination in the regulation of PD-1/PD-L1 in cancer immunotherapy. Mol Ther 29(3):908–919
Lan T, Gao F, Cai Y et al (2025) The protein circPETH-147aa regulates metabolic reprogramming in hepatocellular carcinoma cells to remodel immunosuppressive microenvironment. Nat Commun 16(1):333
Leon-Ferre RA, Goetz MP (2023) Advances in systemic therapies for triple negative breast cancer. BMJ 381:e071674
Leon-Ferre RA, Jonas SF, Salgado R et al (2024) Tumor-Infiltrating Lymphocytes in Triple-Negative Breast Cancer. JAMA 331(13):1135–1144
Li H, Zandberg DP, Kulkarni A et al (2025) Distinct CD8+T cell dynamics associate with response to neoadjuvant cancer immunotherapies. Cancer Cell 43(4):757–775
Liang R, Wang S, Cai Y et al (2025) Circular RNA-mediated inverse prime editing in human cells. Nat Commun 16(1):5057
Liao Y, Yang M, Wang K et al (2022) Deubiquitinating enzyme OTUB1 in immunity and cancer: good player or bad actor? Cancer Lett 526:248–258
Lin Y, Wang Y, Li L, Zhang K (2024) Coding circular RNA in human cancer. Genes Dis 12(3):101347
Liu W, Niu J, Huo Y et al (2025) Role of circular RNAs in cancer therapy resistance. Mol Cancer 24(1):55
Margvelani G, Maquera KAA, Welden JR, Rodgers DW, Stamm S (2025) Translation of circular RNAs. Nucleic Acids Res 53(1):gkae1167
Moini K, Seery T, Nangia C et al (2025) Recurrent pancreatic cancer treated with N-803 and PD-L1 t-haNK followed by an EGFR-targeted nanocell drug conjugate. Oncologist 30(3):oyae267
Murakami S, Olarerin-George AO, Liu JF et al (2025) M6A alters ribosome dynamics to initiate mRNA degradation. Cell 188(14):3728–3743
Palcau AC, Pulito C, De Pascale V et al (2025) CircPVT1 weakens miR-33a-5p unleashing the c-MYC/GLS1 metabolic axis in breast cancer. J Exp Clin Cancer Res 44(1):100
Schmid P, Rugo HS, Adams S et al (2020) Atezolizumab plus nab-paclitaxel as first-line treatment for unresectable, locally advanced or metastatic triple-negative breast cancer (IMpassion130): updated efficacy results from a randomised, double-blind, placebo-controlled, phase 3 trial. Lancet Oncol 21(1):44–59
Shi X, Pang S, Zhou J et al (2024) Bladder-cancer-derived exosomal circRNA_0013936 promotes suppressive immunity by up-regulating fatty acid transporter protein 2 and down-regulating receptor-interacting protein kinase 3 in PMN-MDSCs. Mol Cancer 23(1):52
Tan D, Li G, Li X, Zhai W, Jing L (2026) Curcumin enhances GSDME-mediated pyroptosis to potentiate PD-1/PD-L1 immune checkpoint blockade in colorectal cancer. Front Pharmacol 17:1734653
Wang XQ, Danenberg E, Huang CS et al (2023) Spatial predictors of immunotherapy response in triple-negative breast cancer. Nature 621(7980):868–876
Wang S, Chang CW, Huang J et al (2024) Gasdermin C sensitizes tumor cells to PARP inhibitor therapy in cancer models. J Clin Invest 134(1):e166841
Wei X, Xiang X, Wang H et al (2025) Tumor cell-intrinsic circular RNA circFNDC3B attenuates CD8+T cells infiltration in non-small cell lung cancer. Commun Biol 8(1):711
Xiao S, Ma S, Sun B et al (2024) The tumor-intrinsic role of the m6A reader YTHDF2 in regulating immune evasion. Sci Immunol 9(95):eadl2171
Xu L, Ma X, Zhang X et al (2024) Correction: hsa_circ_0007919 induces LIG1 transcription by binding to FOXA1/TET1 to enhance the DNA damage response and promote gemcitabine resistance in pancreatic ductal adenocarcinoma. Mol Cancer 23(1):16
Zhang Y, Song X, Feng Y et al (2025) The circRNA cEMSY Induces Immunogenic Cell Death and Boosts Immunotherapy Efficacy in Lung Adenocarcinoma. Cancer Res 85(3):497–514
Zhang L, Li Y, Zhou L et al (2023) The m6A reader YTHDF2 promotes bladder cancer progression by suppressing RIG-I-mediated immune response. Cancer Res 83(11):1834–1850
Zhang J, Lv S, Peng X et al (2025) CircERC1 facilitates chemoresistance through inhibiting pyroptosis and remodeling extracellular matrix in pancreatic cancer. Mol Cancer 24(1):185
Zhang W, Liu R, Hu J et al (2025) The deubiquitylase OTUB1 drives gemcitabine resistance in pancreatic cancer by enhancing pyrimidine metabolism through modulating DHODH mRNA stability. Cell Death Dis 16(1):697
Zhou B, Qin Q, Fang Y et al (2024) Exosomes from human bone marrow MSCs alleviate PD-1/PD-L1 inhibitor-induced myocardial injury in melanoma mice by regulating macrophage polarization and pyroptosis. Life Sci 358:123108
Zhu D, Xu R, Huang X et al (2021) Deubiquitinating enzyme OTUB1 promotes cancer cell immunosuppression via preventing ER-associated degradation of immune checkpoint protein PD-L1. Cell Death Differ 28(6):1773–1789

Authors and Affiliations

Honghong Shen[1,2] · Boyu Li[1,2] · Xiaoqian Wen[1,2] · Changqing Zhao[3] · Chen Wang[1,2]

✉ Changqing Zhao
fahyj@126.com

✉ Chen Wang
chenwangshh@126.com

[1] Department of pathology, The Second Clinical Medical College, Shanxi Medical University, Taiyuan 030001, China

[2] Department of Pathology, Ministry of Education, Shanxi Medical University, Taiyuan 030001, China

[3] Department of otorhinolaryngology, The Second Clinical Medical College, Shanxi Medical University, Taiyuan 030001, China